

Deep learning architectures for inference of AC-OPF solutions

Thomas Falconer¹ Letif Mones²

Abstract

We present a systematic comparison between neural network (NN) architectures for inference of AC-OPF solutions. Using fully connected NNs as a baseline we demonstrate the efficacy of leveraging network topology in models by constructing abstract representations of electrical grids in the graph domain for convolutional and graph NNs. The performance of the NN models is compared for both the direct (as regressors predicting optimal generator set-points) and indirect (as classifiers predicting the active set of constraints) approaches and computational gains for obtaining optimal solutions are also presented.

1. Introduction

Electricity market dynamics are generally governed by Optimal Power Flow (OPF) solutions: the computation of (minimal cost) generation dispatch subject to reliability and security constraints of the grid (Wood et al., 2014). The classical OPF formulation (AC-OPF) is a non-linear, non-convex constrained optimisation problem, which, when integrated with day-ahead unit commitment, forms a Mixed-Integer Program known to be NP-hard. Proliferation of intermittent renewable energy sources (e.g. wind and solar) necessitates OPF solutions in near real-time to sustain accurate representation of the system state. This requires solving sequential OPFs at rates unattainable by conventional algorithms.

Generally, AC-OPF is solved using Interior-Point (IP) optimization methods (Wachter & Biegler, 2006), which are expensive given the required computation of the Hessian of the Lagrangian at each iteration. To guarantee suitable rates of convergence, grid operators instead often resort to cheap approximations of OPF, typically DC-OPF – a Linear Program with significantly less control variables and constraints. However, these solutions are predisposed to sub-optimal estimations of locational marginal prices, engendering wasted emissions-intensive electricity generation (Ilic et al., 2006). Extending the OPF objective with generator-wise emissions

¹UCL Energy Institute, London, United Kingdom ²Invenia Labs, Cambridge, United Kingdom. Correspondence to: Thomas Falconer <thomas.falconer.19@ucl.ac.uk>.

costing furthers the computational burden, hence enabling fast computation of AC-OPF not only facilities renewable energy generation, but is a direct method for climate change mitigation.

Applications of machine learning (ML) to OPF typically use regression techniques to directly infer the OPF solution from grid parameters, bypassing conventional solvers (Guha et al., 2019). However, since it is not a smooth function of the inputs, this approach necessitates training on relatively large data sets to obtain acceptable accuracy. Further, ensuring constraint satisfaction with regression methods is challenging hence feasibility is not necessarily guaranteed, let alone optimality, posing security risks to the grid. It is more pragmatic therefore to augment the IP method by initialising the solver with the inferred optimal solution, a so-called warm-start (Baker, 2019), and use a (meta-)loss function corresponding directly to the time complexity, minimising computational burden (Jamei et al., 2019).

Alternatively, the optimal active set (Misra et al., 2018) or the binding status of each constraint can be inferred (Robson et al., 2019) using classification. Although the number of constraints is exponential in system size (Deka & Misra, 2019), typically only a fraction constitutes the active set, thus a reduced problem can be formulated whilst preserving the objective. Security risks associated with false negatives can be avoided by iteratively solving the (cheap) reduced OPF and adding violated constraints until all those of the full problem are satisfied. The cost of this procedure can also be minimised via meta-optimisation by directly encoding the time complexity into the (meta-)loss function and optimising the weights accordingly (Robson et al., 2019).

In each case, it is crucial to use model architectures which maximise predictive performance. The field typically employs fully connected models (FCNNs), however CNNs (Chen & Tate, 2020) and GNNs (Owerko et al., 2019) have recently been investigated to exploit spatial dependencies within the electrical grid. This paper addresses contentions throughout literature of the most suitable modelling frameworks for OPF by offering a systematic comparison between these architectures, and between the regression and classification methods. Two input domains are studied: (1) only load variables, to exclusively mimic fluctuations in demand and (2) the entire set of grid parameters, to reflect the sea-

sonality of all grid components and to evaluate the utility of the architectures in (more realistic) high-dimensional scenarios. Experiments are carried out using synthetic grids from Power Grid Lib (Babaeinejadsarookolaee et al., 2019). We believe our work can facilitate the transition toward a clean and efficient power grid – an important contribution to tackling climate change.

2. Methods

The electrical grid can be represented as an un-directed graph $\mathbb{G} = (\mathcal{V}, \mathcal{E})$ with a set of $|\mathcal{V}|$ number of nodes (buses) and $|\mathcal{E}|$ number of edges (transmission lines). The grid control variables are the set of active and reactive nodal loads, maximum active and reactive power outputs of generators, line thermal ratings and the reactance and resistance of each transmission line. Hereafter we refer to the two studied domains of the control variables as: (1) only load variables $\Phi = \Phi_{\text{load}}$ and (2) all grid parameters $\Phi = \Phi_{\text{all}}$.

To maintain validity of the constructed data sets, we generate samples within prescribed boundaries around the Power Grid Lib defaults: $\pm 15\%$ for nodal active load and $\pm 10\%$ for all remaining parameters. On account of demonstrated computational efficiency relative to conventional Uniform scaling methods, we adopt a Random Walk Metropolis-Hastings-based sampling technique whereby steps are taken through normalised space subject to an isotropic Gaussian proposal distribution $\mathcal{N}(\mathbf{x}^*, \alpha \mathbf{I})$, centred on the current system state \mathbf{x}^* with step size α , only accepting AC feasible candidates (Falconer, 2020). AC-OPF solutions were found using `PowerModels.jl` (Coffrin et al., 2017) in combination with the `IPOPT` solver (Wachter & Biegler, 2006).

For an arbitrary input sample \mathbf{x} the regression objective is to infer the set of optimal primal variables (phase angles and active power injections), indicative of the minimum information required for the warm-start. Defining $\mathcal{G} \subset \mathcal{V}$ as the set of generators, the regressor learns the *true* AC-OPF mapping defined by $\Omega : \mathbb{R}^{|\Phi|} \mapsto \mathbb{R}^{|\mathcal{V}|+|\mathcal{G}|}$ by parameterising a neural network $\hat{\Omega}$ with parameters Θ and minimising the mean-squared error (MSE) between the ground-truths $\mathbf{y} = \Omega(\mathbf{x})$ and the inferred solution $\hat{\mathbf{y}} = \hat{\Omega}(\mathbf{x}, \Theta)$.

The classification setting determines the binding status of each constraint in \mathcal{C} , the subset of inequality constraints which change binding status at least once in the training set (hereafter referred to as non-trivial constraints). We define $\mathbf{y} \in \mathbb{R}^{|\mathcal{C}|}$ as a binary vector representing an enumeration of the set of constraints. The classifier learns the mapping $\Psi : \mathbb{R}^{|\Phi|} \mapsto \mathbb{R}^{|\mathcal{C}|}$ by minimising the binary cross-entropy loss (BCE) between the ground-truths $\mathbf{y} = \Psi(\mathbf{x})$ and the predicted probabilities $\hat{\mathbf{y}} = \hat{\Psi}(\mathbf{x}, \Theta)$.

We first construct a baseline FCNN designed to operate on data in vector format, hence lacking sufficient relational

inductive bias to exploit any underlying structure. Network topology can be expressed in the graph domain using the (weighted) binary adjacency matrix. For CNNs with only load variables as input, each parameter can be represented by a vector of length $|\mathcal{V}|$ and subsequently combined into a 3D tensor such that $\mathbf{x} \in \mathbb{R}^{|\mathcal{V}| \times 1 \times |\Phi|}$. For all grid parameters, those relevant to nodes Φ^V or edges Φ^E can be constructed into diagonal or off-diagonal matrices, respectively such that the input is defined as $\mathbf{x} \in \mathbb{R}^{|\mathcal{V}| \times |\mathcal{V}| \times |\Phi|}$.

For GNNs, we investigate both spectral and spatial convolutions, the latter of which are typically constrained to operate on node features and a 1D set of edge features. We overcome this limitation by encoding edge features as node features by concatenating structures akin to that mentioned above, such that the input is $\mathbf{x} \in \mathbb{R}^{|\mathcal{V}| \times (|\Phi^V| + |\Phi^E| |\mathcal{V}|)}$. Although spatial graph convolutions ordinarily permit multi-dimensional edge features, enhanced performance was observed empirically using an input structure akin to that defined here.

Spectral graph convolutions operate in the Fourier domain; input signals are passed through parameterised functions of the normalised Laplacian, exploiting its positive-semidefinite property. Given this procedure has $\mathcal{O}(|\mathcal{V}|^3)$ time complexity, we investigate two spectral layers, namely ChebConv (Kipf & Welling, 2016) and GCNConv (Defferrard et al., 2016), which reduce the computational cost by approximating filter functions using Chebyshev polynomials of the eigenvalues up to the K -th order, avoiding expensive full eigendecomposition of the Laplacian. GCNConv constrains the layer-wise convolution to first-order neighbours ($K = 1$), lessening overfitting to particular localities.

Spatial graph convolutions are instead directly performed in the graph domain, reducing time complexity whilst minimising information loss. For a given node, SplineConv computes a linear combination of its features together with those of its K -th order neighbours, weighted by a kernel function using the product of parameterised B-spline basis functions (Fey et al., 2017). The local support property of B-splines reduces the number of parameters, enhancing the computational efficiency of the operator.

Each graph layer (ChebConv, GCNConv and SplineConv) was used to construct a unique GNN, hereafter referred to as CHNN, GCN and SNN, respectively. Parameters were optimised using ADAM (Kingma & Ba, 2014) with learning rate initialised at $\eta = 10^{-4}$. Hidden layers were applied with BatchNorm and a ReLU activation function; dropout (with probability of 0.4) was applied to fully-connected layers. CNNs were constructed using 3×3 kernels, 2×2 max-pooling layers, zero-padding and a stride length of 1. For CHNN and SNN, K was set to 5. Hyper-parameters were tuned iteratively, to construct models, where for each case the number of weights was in the same order of magnitude to facilitate a fair comparison of performance.

3. Results

We generated 10k samples for several synthetic grids (Table 1). Less unique active sets were uncovered using only load variables since without altering the other grid parameters, changes in system state are much less profound, rendering homogeneity amongst congestion regimes. For the 300-ieee case, this is capped at the number of samples, implying that even 10k samples restricts convergence to the *true* parameter distribution for larger grids. The additional complexity of using all grid parameters is highlighted by the larger input domains $\text{dim}(\Phi)$ in addition to the greater cardinalities of non-trivial constraints $|\mathcal{C}|$. Data sets were subsequently split into training, validation and test sets with a ratio of 80:10:10.

Table 1. Grid characteristics and number of unique active sets for different AC-OPF cases, using 10k samples.

| Case | Only Load: $\Phi = \Phi_{\text{load}}$ | | | All Parameters: $\Phi = \Phi_{\text{all}}$ | | |
|--------------|--|-----------------|---------------|--|-----------------|---------------|
| | $\text{dim}(\Phi)$ | $ \mathcal{C} $ | # Active Sets | $\text{dim}(\Phi)$ | $ \mathcal{C} $ | # Active Sets |
| 73-ieee-rts | 146 | 28 | 1008 | 660 | 60 | 2902 |
| 118-ieee | 236 | 31 | 437 | 864 | 66 | 6649 |
| 162-ieee-dtc | 322 | 58 | 1805 | 1102 | 92 | 6026 |
| 300-ieee | 600 | 143 | 9803 | 1773 | 201 | 10000 |

Regression performance is depicted by the average (test set) MSE for five independent runs (Table 2); each GNN outperforms FCNN and CNN, in some cases by an order of magnitude. Relative performance is more overt using only load given the lower input dimensionality, however, we still see performance enhancements in the more complex all parameter setting. SNN typically outperforms GCN and CHNN, possibly due to the information loss via spectral node embedding. This, combined with reduced training times in virtue of the computational efficiency of the B-spline kernel functions, alludes to better scaling to larger systems. We observe no significant performance enhancements using CNN, which was expected since the non-Euclidean data structures are deprived of the geometric priors on which the convolution operator relies. Anomalous cases of reduced error can be attributed to the coincidental unearthing of structural information within the receptive fields when convolving over the (weighted) adjacency matrices.

Table 2. Average test set MSE values of regression models.

| Case ($\Phi = \Phi_{\text{load}}$) | FCNN | CNN | GCN | CHNN | SNN | |
|--------------------------------------|-----------|-------|-------|--------------|-------|--------------|
| 73-ieee-rts | 10^{-4} | 6.613 | 7.625 | 0.556 | 0.612 | 0.527 |
| 118-ieee | 10^{-4} | 2.171 | 3.042 | 0.306 | 0.334 | 0.329 |
| 162-ieee-dtc | 10^{-3} | 9.492 | 6.026 | 3.341 | 3.039 | 2.145 |
| 300-ieee | 10^{-2} | 3.654 | 5.973 | 2.283 | 2.156 | 1.948 |
| Case ($\Phi = \Phi_{\text{all}}$) | FCNN | CNN | GCN | CHNN | SNN | |
| 73-ieee-rts | 10^{-3} | 4.916 | 5.241 | 2.011 | 1.953 | 1.247 |
| 118-ieee | 10^{-3} | 2.621 | 3.487 | 0.396 | 0.450 | 0.372 |
| 162-ieee-dtc | 10^{-2} | 2.783 | 4.585 | 1.411 | 1.682 | 1.229 |
| 300-ieee | 10^{-1} | 1.293 | 1.466 | 0.723 | 0.711 | 0.574 |

Classification performance is reported in terms of average (test set) recall and precision, in addition to BCE, to see how

each model balances the trade-off between false positives (FPs) and false negatives (FNs). GNNs again outperform FCNN and CNN in each case, subject to each metric (Table 3). Interestingly, we observe a greater precision than recall in virtually every instance, implying the BCE objective is more sensitive to FPs, which is unfavourable given the computational cost of omitting *true* binding constraints from the reduced problem (FNs). This implies the loss function is misaligned with the desired objective and should be altered to bias the reduction of FNs.

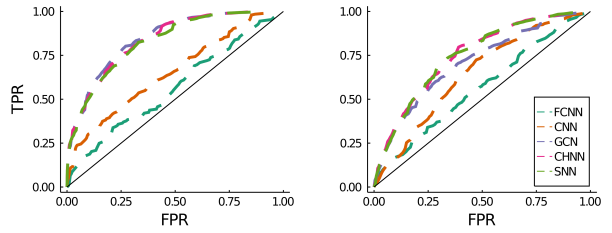


Figure 1. ROC curves for each classification model (118-ieee system) using only load (left) and all parameters (right) as input.

Using the 118-ieee system as a case study to visualise the ROC curves for each model (Figure 1), we observe that GNNs are superior irrespective of classification threshold. For many of the binary classifications, GNNs demonstrated AUCs surpassing 0.9, whereas FCNN and CNN often reported AUCs less than 0.5, i.e. worse than random.

Finally, we report the average (test set) computational gain realised for the warm-start and reduced problem, using all grid parameters as a case study (Table 4). In both settings, the models that provide more accurate inference (GNNs) engender superior gains. The similar or greater performance of the reduced problem relative to the warm-start implies that this method is preferable overall, as we could achieve greater gains merely by reducing the number of FNs with a more sophisticated objective function.

4. Conclusion

Our systematic comparison of NN architectures for direct and indirect inferences of AC-OPF solutions, as well as methods for augmenting the IP solver, has highlighted the importance of predictive accuracy in reducing the computational cost of AC-OPF with ML, essential for minimising emissions in the electricity market. We demonstrated the utility of explicitly incorporating network topology in the learning process using GNNs and concluded the gains of the reduced problem allude to better scaling to larger grids. In future work, we will investigate more sophisticated objectives to bias the optimisation towards a reduction in FNs, and leverage the capacity of GNNs to supplement the meta-optimisation technique proposed by Robson et al. (2019).

Table 3. Average BCE, recall and precision of classification models.

| Case ($\Phi = \Phi_{\text{load}}$) | BCE | | | | | Recall | | | | | Precision | | | | |
|--------------------------------------|-------|-------|-------|--------------|--------------|--------|-------|--------------|--------------|--------------|-----------|-------|--------------|--------------|--------------|
| | FCNN | CNN | GCN | CHNN | SNN | FCNN | CNN | GCN | CHNN | SNN | FCNN | CNN | GCN | CHNN | SNN |
| 73-ieee-rts | 0.183 | 0.158 | 0.064 | 0.061 | 0.057 | 0.724 | 0.774 | 0.854 | 0.843 | 0.865 | 0.928 | 0.935 | 0.964 | 0.946 | 0.976 |
| 118-ieee | 0.193 | 0.179 | 0.041 | 0.039 | 0.052 | 0.631 | 0.658 | 0.772 | 0.738 | 0.792 | 0.942 | 0.875 | 0.957 | 0.929 | 0.946 |
| 162-ieee-dtc | 0.235 | 0.214 | 0.093 | 0.089 | 0.084 | 0.682 | 0.675 | 0.764 | 0.767 | 0.761 | 0.773 | 0.782 | 0.857 | 0.871 | 0.864 |
| 300-ieee | 0.157 | 0.163 | 0.111 | 0.107 | 0.115 | 0.611 | 0.582 | 0.683 | 0.678 | 0.664 | 0.775 | 0.791 | 0.874 | 0.882 | 0.879 |

| Case ($\Phi = \Phi_{\text{all}}$) | BCE | | | | | Recall | | | | | Precision | | | | |
|-------------------------------------|-------|-------|-------|--------------|--------------|--------|-------|--------------|-------|--------------|-----------|-------|-------|--------------|--------------|
| | FCNN | CNN | GCN | CHNN | SNN | FCNN | CNN | GCN | CHNN | SNN | FCNN | CNN | GCN | CHNN | SNN |
| 73-ieee-rts | 0.263 | 0.247 | 0.115 | 0.123 | 0.111 | 0.602 | 0.597 | 0.642 | 0.699 | 0.724 | 0.893 | 0.874 | 0.89 | 0.892 | 0.921 |
| 118-ieee | 0.224 | 0.206 | 0.104 | 0.101 | 0.098 | 0.532 | 0.614 | 0.685 | 0.674 | 0.676 | 0.846 | 0.833 | 0.873 | 0.891 | 0.86 |
| 162-ieee-dtc | 0.187 | 0.194 | 0.136 | 0.127 | 0.131 | 0.491 | 0.482 | 0.538 | 0.523 | 0.552 | 0.823 | 0.835 | 0.879 | 0.886 | 0.873 |
| 300-ieee | 0.195 | 0.201 | 0.128 | 0.121 | 0.119 | 0.587 | 0.583 | 0.635 | 0.638 | 0.642 | 0.794 | 0.801 | 0.847 | 0.845 | 0.859 |

Table 4. Average computational gain for direct (warm-start) and indirect (reduced problem) approaches.

| Case (direct) | FCNN | CNN | GCN | CHNN | SNN |
|---------------|---------|---------|--------------|--------------|---------------|
| 73-ieee-rts | 17.58 | 15.76 | 21.65 | 21.18 | 21.43 |
| 118-ieee | 14.38 | 15.92 | 17.27 | 16.57 | 17.09 |
| 162-ieee-dtc | -133.74 | -125.79 | -96.76 | -93.79 | -90.64 |
| 300-ieee | 12.20 | 11.67 | 17.31 | 17.56 | 16.38 |

| Case (indirect) | FCNN | CNN | GCN | CHNN | SNN |
|-----------------|--------|--------|--------------|--------------|--------------|
| 73-ieee-rts | -13.82 | -11.91 | -4.26 | -2.60 | -1.31 |
| 118-ieee | 21.17 | 22.91 | 27.06 | 26.44 | 25.75 |
| 162-ieee-dtc | -38.29 | -25.08 | -10.87 | -9.10 | -12.26 |
| 300-ieee | 13.24 | 12.83 | 17.84 | 16.90 | 17.73 |

References

Babaeinejadsarookolaee, S., Birchfield, A., Christie, R. D., Coffrin, C., DeMarco, C., Diao, R., Ferris, M., Flisounakis, S., Greene, S., Huang, R., Josz, C., Korab, R., Lesieutre, B., Maeght, J., Molzahn, D., Overbye, T., Panciatici, P., Park, B., Snodgrass, J., and Zimmerman, R. The power grid library for benchmarking ac optimal power flow algorithms. 2019.

Baker, K. Learning warm-start points for ac optimal power flow, 2019.

Chen, L. and Tate, J. E. Hot-starting the ac power flow with convolutional neural networks, 2020.

Coffrin, C., Bent, R., Sundar, K., Ng, Y., and Lubin, M. Powermodels.jl: An open-source framework for exploring power flow formulations, 2017.

Defferrard, M., Bresson, X., and Vandergheynst, P. Convolutional neural networks on graphs with fast localized spectral filtering, 2016.

Deka, D. and Misra, S. Learning for dc-opf: Classifying active sets using neural nets. 2019 IEEE Milan PowerTech, pp. 1–6, 2019.

Falconer, T. Reducing the computational cost of ac optimal power flow with geometric deep learning, 2020.

Fey, M., Lenssen, J. E., Weichert, F., and Müller, H. Splinecnn: Fast geometric deep learning with continuous b-spline kernels, 2017.

Guha, N., Wang, Z., Wytock, M., and Majumdar, A. Machine learning for ac optimal power flow, 2019.

Ilic, M. D., Lang, J. H., Litvinov, E., and Luo, X. The critical role of computationally robust ac optimal power flow in reliable and efficient reactive power/voltage dispatch. In 2006 IEEE PES Power Systems Conference and Exposition, pp. 689–698, 2006.

Jamei, M., Mones, L., Robson, A., White, L., Requeima, J., and Ududec, C. Meta-optimization of optimal power flow. 2019.

Kingma, D. P. and Ba, J. Adam: A method for stochastic optimization, 2014.

Kipf, T. N. and Welling, M. Semi-supervised classification with graph convolutional networks, 2016.

Misra, S., Roald, L. A., and Ng, Y. Learning for constrained optimization: Identifying optimal active constraint sets. Optimization and Control, 2018.

Owerko, D., Gama, F., and Ribeiro, A. Optimal power flow using graph neural networks, 2019.

Robson, A., Jamei, M., Ududec, C., and Mones, L. Learning an optimally reduced formulation of opf through meta-optimization. 2019.

Wachter, A. and Biegler, L. On the implementation of an interior-point filter line-search algorithm for large-scale nonlinear programming. Mathematical programming, 106:25–57, 2006.

Wood, A. J., Wollenberg, B. F., and Sheble, G. B. Power generation, operation, and control. Wiley InterScience, 2014.